EAST EUROPEAN JOURNAL OF PHYSICS. 2. 169-178 (2026)
DOI:10.26565/2312-4334-2026-2-17 ISSN 2312-4334

DFT INVESTIGATION OF ELECTRONIC, ELASTIC, AND TRANSPORT PROPERTIES, AND EVALUATION OF LATTICE THERMAL CONDUCTIVITY OF THE HALF-HEUSLER ALLOY RuAsNb

Aziza Boutouta[1], Amor Bouaricha[2,5], F. Zenikheri[3,7], Zeyneb Bordjiba[4], Rabie Amraoui[3,4], Salim Kadri[5,6], Walid Bendjeddou[6], Salah Aguib[6]

[1]*Center of Research in Mechanics CRM, Po. Box 73 B, 25021, Constantine, Algeria*
[2]*University of Ghardaia Scientific Zone, PO Box 455, Ghardaia, 47000, Algeria*
[3]*Higher Normal School of Technological Education, Skikda, 21000, Algeria*
[4]*Material Physics Laboratory - L2PM, 8 May 1945 University of Guelma, Algeria*
[5]*Industrial Mechanics Laboratory (LMI), Badji Mokhtar—Annaba University, P.O. Box 12, Annaba, 23000, Algeria*
[6]*Dynamic of Engines and Vibroacoustic Laboratory (LDMV), University of M'hamed Bouguerra, Boumerds, 35000, Algeria*
[7]*Laboratory of the Active Components and Materials, Larbi Ben M'Hidi University, Oum El Bouaghi, 04000, Algeria*
**Corresponding Author email: amraoui.rabie@yahoo.com*
Received September 25, 2025; revised April 28, 2026; accepted May 8, 2026

In this study, we employed the Full-Potential Linearized Augmented Plane Wave (FP-LAPW) method, as implemented in Wien2k, to perform a comprehensive investigation of the structural, electronic, and thermoelectric properties of RuAsNb. The electronic band structure was calculated using the TB-mBJ exchange-correlation potential, resulting in an energy gap that is in close agreement with the available experimental data. Furthermore, our analysis revealed favorable optical properties, highlighting the material's potential for applications across the infrared, visible, and ultraviolet regions of the electromagnetic spectrum. We also evaluated the thermoelectric performance of RuAsNb by analyzing key parameters, including the Seebeck coefficient, electrical conductivity, thermal conductivity, and power factor. The results indicate that holes are the dominant charge carriers, confirming the p-type semiconducting nature of RuAsNb. In addition, the effect of chemical potential variations on these thermoelectric properties was examined, providing valuable insights into their temperature-dependent behavior. To ensure the robustness of our findings, a comparative study using different exchange–correlation potentials was conducted, which further validated the consistency of the results. The promising thermoelectric performance of RuAsNb suggests its suitability as a potential candidate for next-generation energy conversion devices and photovoltaic applications. Moreover, the estimation of the lattice thermal conductivity using the Slack model reinforces the reliability of our predictions and provides valuable insights for future research. Overall, this work contributes to a deeper understanding of the potential of RuAsNb in advanced energy materials.
Keywords: *Half Heusler; DFT; Structural property; Anisotropic; Optical properties; Figure of merit*
PACS: 71.15.Mb; 71.20.-b; 71.55.Ak; 72.20.Pa

1. INTRODUCTION

Currently, scientists place paramount importance on thermoelectric performance due to its ability to directly convert waste thermal energy into clean and non-polluting electrical energy **[1]**. This growing interest is driven by the depletion of fossil fuel reserves and the significant environmental impacts associated with their widespread use. Consequently, the search for new thermoelectric materials has become a major priority in the development of alternative energy resources.

Among the materials investigated for this purpose are Half-Heusler (HH) compounds, a class of materials distinguished by several attractive physical properties, including elastic stability, high melting temperature, a high thermoelectric power factor, a favorable figure of merit, and stable thermal behavior.

In recent years, Half-Heusler (HH) compounds have attracted considerable attention due to their excellent thermoelectric performance and low thermal conductivity. In our recent study, we focused on Half-Heusler compounds containing X elements such as Co, Rh, and Ir, combined with MnAs **[1]**. To characterize these compounds, we employed Density Functional Theory (DFT), a powerful method for modeling material properties. Using DFT, we systematically investigated the structural, elastic, thermal, and transport properties of these compounds. This comprehensive approach provided in-depth insights into their physical behavior, laying the foundation for a better understanding of their thermoelectric performance.

In this new study, our focus has shifted to the Half-Heusler compound RuAsNb, which has been mentioned in previous works, although these studies did not investigate the parameters we address. For instance, Zhenzhen Feng *et al.* **[2]** examined a set of 75 Half-Heusler-type compounds, using electronic structure as a criterion for identifying promising thermoelectric materials. This approach enabled the exploration of a wide range of compounds and the assessment of their potential based on their electronic structure characteristics.

The same authors, Zhenzhen Feng *et al.* **[3]**, conducted another noteworthy study in which they explored the concept of resonance in stoichiometrically ordered Half-Heusler compounds. They employed first-principles phonon calculations and thermal conductivity analyses to identify materials exhibiting low thermal conductivity.

Cite as: A. Boutouta, A. Bouaricha, F. Zenikheri, Z. Bordjiba, R. Amraoui, S. Kadri, W. Bendjeddou, S. Aguib, East Eur. J. Phys. 2, 169 (2026), https://doi.org/10.26565/2312-4334-2026-2-17

A more recent contribution was reported by Fatiha Cherifi *et al.* **[4]**, entitled *"Thermoelectric transport parameters of p-type RuVAs and RuNbAs Heusler alloys."* In this work, the authors successfully characterized the semiconducting nature of both RuVAs and RuNbAs. They also presented the electronic band structures and calculated the elastic constants. However, they did not evaluate several essential mechanical parameters required for a comprehensive understanding of these compounds, such as the bulk modulus, shear modulus, Young's modulus, Poisson's ratio, hardness, Zener anisotropy factor, Cauchy pressure, and the Pugh ratio. These parameters constitute the core of our research objectives.

The aim of this study is to conduct a comprehensive investigation of the structural, elastic, and thermoelectric properties of the RuAsNb compound using *ab initio* calculations. We evaluate the elastic stability of this material and determine a comprehensive set of mechanical parameters to gain deeper insight into its intrinsic behavior. By employing the BoltzTraP code, we solve the Boltzmann transport equation to analyze the material's transport properties. This approach enables the detailed evaluation of key parameters such as the Seebeck coefficient, as well as the electronic contributions to electrical and thermal conductivities.

These parameters are essential for a thorough understanding of the thermoelectric performance of the compound, particularly in terms of the power factor and the figure of merit, which are critical indicators of its efficiency in converting thermal energy into electrical energy. Furthermore, we apply the Slack model to investigate the temperature dependence of lattice thermal conductivity—an aspect not previously addressed particularly in the work of Fatiha Cherifi et al. [4], where only the ambient-temperature value was reported.

In addition, while Fatiha Cherifi *et al.* **[4]** limited their analysis to thermoelectric properties as a function of temperature. Our approach goes further by presenting detailed variations in thermoelectric performance as a function of chemical potential over a wide range of temperatures. This provides a deeper and more comprehensive understanding of the material's transport behavior.

2. COMPUTATIONAL METHOD

We employed the WIEN2k software **[5]** to calculate the electronic structure of the cubic-phase RuAsNb compound within the framework of Density Functional Theory (DFT) **[6].** The full-potential linearized augmented plane wave (FP-LAPW) method was used in conjunction with the generalized gradient approximation in the Wu–Cohen scheme (GGA-WC) for the exchange–correlation energy. A total of 3000 k-points were used for integration over the irreducible Brillouin zone, with a plane-wave cutoff parameter of RKmax=8RK.

Using the eigenvalues and eigenvectors obtained at these k-points, further analyses were performed. The Half-Heusler compound RuAsNb crystallizes in the cubic C_{1b} structure, as illustrated in Figure 1. In this structure, the Ru atom occupies the 4a site (0.25, 0.25, 0.25), the As atom occupies the 4b site (0.5, 0.5, 0.5), and the Nb atom occupies the 4c site (0, 0, 0), according to the Wyckoff positions **[7].**

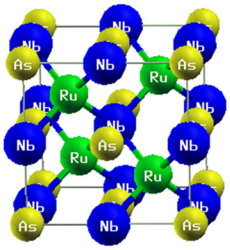

Figure 1. Computed crystal structure of RuAsNb

3. RESULTS AND DISCUSSION

3.1. Electronic Band Structures and Density of State (DOS)

The electronic band structures of the RuAsNb compound, calculated using the generalized gradient approximation (GGA-PBE), are displayed in Figure 2, providing a detailed analysis along the symmetry directions. It is evident that this compound exhibits semiconductor behavior with a direct band gap **[8].** The calculated band energies are offering essential quantitative values for evaluating its electronic properties. The computed bandgap is found to be 0.23 eV and indirect in nature. Additionally, we observe a notably flat valence band, which suggests a significant effective mass for the charge carriers. This characteristic is advantageous for thermoelectric performance, as it facilitates improved carrier mobility.

To further elucidate the electronic structure of the compound under study, we calculated both the total density of states (DOS) and the partial density of states (PDOS). These results are presented in Figure 2 (b) covering an energy range from -10 to 10 eV. The PDOS plot for RuAsNb indicates that the lowest valence states in the range of -10 to -7.5 eV primarily originate from the As-p states, with a very minimal contribution from the other atoms present in the compound. Figure 2(b) illustrates the total and partial electronic density of states for RuAsNb. It is clear that the valence band, located between -2 and -5.90 eV, is predominantly composed of Ru-d states, with a contribution from Nb-d states. The Ru-d states are particularly dominant near the Fermi level, while the contribution from As-p states remains minimal. In contrast, the conduction band in the range of 0 to 5 eV is mainly dominated by Nb-d states, with a lesser contribution from Ru-d states **[9].** The As-p states exhibit very little participation in this energy range, although the contributions from all three

atomic states become more balanced in the conduction band between 5 and 9 eV. Overall, the high electronic density of states near the Fermi level in this compound suggests a significant potential for a large Seebeck coefficient, thereby suggesting a high thermoelectric power factor. These findings will be further explored in the subsequent subsection, where we will discuss the implications of these electronic characteristics on the thermoelectric performance of RuAsNb.

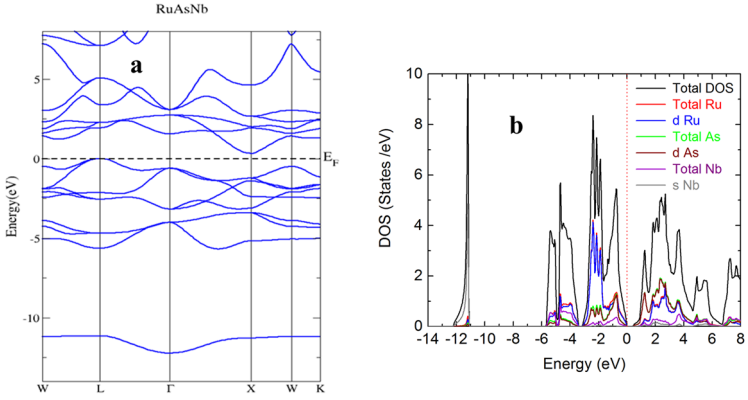

Figure 2. (a) Computed band structure of RuAsNb (b) density of states for RuAsNb

3.2. Elastic properties

The objective of analyzing the mechanical behavior of a new material is to understand its response to solicitations. It is clear that, in physics, elasticity is the property of a solid material to regain its original shape after being deformed. The elastic constants of the RuAsNb alloy were calculated using the Thomas Charpin method **[10],** implemented in the Wien2k code. We will compare our results with those of Fatiha Cherifi et al **[10].** It is noteworthy that the calculated elastic constants adhere to the Born-Huang criteria for mechanical stability **[11]:** $C_{44} > 0$, $C_{11} - C_{12} > 0$, $C_{11} + 2\,C_{12} > 0$, and C_{12} must be less than C_{11}.

To describe the mechanical behavior of these materials based on the *Cij* constants, elastic parameters such as the shear modulus G, Young's modulus E and Poisson's ratio ν are evaluated using the Voigt-Reuss-Hill approximation **[12]** at pressure $P = 0$, where the indices R and V for the compressibility modulus and shear modulus are associated with the Voigt and Reuss approximations, respectively. For cubic systems, these elastic parameters are calculated using the following expressions:

$$B = \frac{C_{11}+2.C_{12}}{3}, \tag{1}$$

$$G = \frac{G_V+G_R}{2}, \tag{2}$$

$$G_V = \frac{(C_{11}-C_{12}+3.C_{44})}{5}, \tag{3}$$

$$G_R = \frac{5.C_{44}(C_{11}-C_{12})}{4.C_{44}+3(C_{11}-C_{12})}, \tag{4}$$

$$E = \frac{9.B.G}{(3.B+G)}, \tag{5}$$

$$\nu = \frac{3.B-E}{6.B}. \tag{6}$$

We observe that these constants satisfy the cubic stability condition, i.e., $C_{12} < B < C_{11}$, confirming that this alloy is elastically stable.

The results obtained for this compound are given in Table 1, and we note the absence of theoretical values from the literature. The bulk modulus B provides indications about the hardness of the material; the larger it is, the harder the material. The compressibility module value for this Half-Heusler compound is high ($B > 30\ GPa$), indicating low compressibility **[13]**. Therefore, this alloy can be classified as relatively hard, capable of withstanding changes in volume and shape under ambient conditions. We observe that the shear modulus of the studied alloy is lower than the bulk modulus, suggesting that this alloy exhibits higher resistance to volumetric compression than to shape change.

We can differentiate the brittleness and ductility of a material based on the Pugh ratio (B/G) **[13]**, Thus, if ($B/G > 1.75$), the material is ductile; otherwise, if ($B/G < 1.75$), the material is hard and brittle. According to Table 1, the value of this ratio is greater than 1.75, so we can consider that our alloy is ductile. The Young's modulus E is an indicator of a material's stiffness. The higher the Young's modulus for a given material, the stiffer it is. This property measures a material's ability to resist elastic deformation under applied stress, providing crucial insights into its structural strength

and response to mechanical stress. The obtained value of Young's modulus *E* is relatively high, demonstrating the rigid characteristic of our studied alloy.

We can also assess the hardness of this alloy, as it is a mechanical property that provides information about the plasticity, elasticity, and strength of materials. In our study, we adopted the Vickers microhardness model using the following expression provided by Tian et al **[14]**:

$$H_V = 0.92 \cdot \left(\frac{G}{B}\right)^{1,137} \cdot G^{0,703}. \quad (7)$$

In conclusion, based on Table 1, we observe that the studied material exhibits favorable hardness characteristics, making it a suitable choice for small electronic or mechanical components.

The knowledge of elastic constants has also allowed us to deduce other mechanical quantities, such as anisotropy A , Cauchy coefficient CP and melting temperature.

The Zener anisotropy factor measures the degree of anisotropy in solids. A material is considered completely isotropic if $A=1$, while any value below or above "1" indicates the anisotropy of the material. It is determined by the following relation **[15]:**

$$A = {}^{2.C_{44}}/_{(C_{11}-C_{12})}. \quad (8)$$

In our compounds, a Zener anisotropy factor different from 1 implies that the compound is anisotropic. We also know that when is close to 1, it indicates maximum stiffness along the <111> cube diagonal, which is the case for our compound.

Determining the Cauchy pressure (*CP*) is used to assess the nature of atomic bonding in metals and compounds, whether they exhibit brittle or ductile characteristics **[16].**

$$CP = C_{12} - C_{44}. \quad (9)$$

For our alloy, the Cauchy pressure has a positive value, indicating the ductile and metallic nature of our material. We have also calculated the melting temperature from the elastic constants using the following equation **[17]**:

$$T_m(K) = [553 + (5.911) \cdot C_{12}] \mp 300 \quad (10)$$

The Debye temperature (θD) provides essential insights into the properties of a solid material in response to temperature, being linked to the upper limit of phonon frequencies. The calculation of the Debye temperature using elastic constants is a reliable process, based on the following equation **[16, 17]:**

$$\theta_D = \frac{h}{k_B}\left[\frac{3}{4.\pi}\left(\frac{N_A.\rho}{M}\right)\right]^{\frac{1}{3}} \mathrm{V}_m \quad (11)$$

Where N_a is the Avogadro number; *M* is molar mass; ρ is the density; h is the Planck constant and k_B is Boltzmann constant. V_m is the sound mean velocity given by:

$$\mathrm{V}_m = \left[\frac{1}{3}\left(\frac{2}{V_t^3} + \frac{1}{V_l^3}\right)\right]^{-\frac{1}{3}}. \quad (12)$$

Where: $V_l = \left(\frac{3B+4G}{3\rho}\right)^{\frac{1}{2}}$, $V_t = \left(\frac{G}{\rho}\right)^{\frac{1}{2}}$ represent the longitudinal sound velocity, and the transverse sound propagation velocity, respectively.

The results of the elastic parameters and behavior of this compound are mentioned below in Table 1.

Table 1. elastic constants (C_{11},C_{12} ,C_{44}) GPa, Bulk Modulus (B) GPa, Shear Modulus (G) GPa, Young Modulus (E) GPa, Poisson ratio (ν), (B/G) Ratio, Micro Hardness (H), The Anisotropy A , Cauchy Coefficient CP , Melting Temperature (T_m) in °K, Debye temperature (θ_D) in °K

RuAsNb	C_{11}	C_{12}	C_{44}	B	G	E	ν	B/G	H	A	CP	$T_m \pm 300$	θ_D
This work	268.5	172.6	116.5	204.56	89.06	233.33	0.34	2.29	8.39	2.429	56.1	1573.23	388.61
Other work [4]	250.951	158.761	96.734	-	-	-	-	-	-	-	-	-	-

The study of the elastic properties of three-dimensional (3D) surfaces provides a clear visualization and a comprehensive explanation of the anisotropic behavior of mechanical modules.

The dependence on the crystallographic direction of the bulk modulus *B*, Young's modulus *E* and shear modulus *G* is calculated using the following expressions **[15]**:

$$\begin{cases} \frac{1}{B} = (S_{11} + 2.S_{12})(l_1^2 + l_2^2 + l_3^2) \\ \frac{1}{E} = S_{11} - 2.\left(S_{11} - S_{12} - \frac{1}{2}S_{44}\right)(l_1^2 l_2^2 + l_2^2 l_3^2 + l_3^2 l_1^2) \\ \frac{1}{G} = S_{44} - 4\left(S_{11} - S_{12} - \frac{1}{2}S_{44}\right)(sin^2\theta \cdot cos^2\theta + 0.125sin^4)(1 - cos4\varphi) \end{cases} \quad (13)$$

There S_{ij} are the elements of the matrix of elastic compliance constants, which are obtained from the inverse of the matrix of elastic constants; ($S_{ij} = C_{ij}^{-1}$), and l_1, l_2, l_3 are the direction cosines along the x, y, and z axes. We found the S_{ij} respectively: $S_{11} = 0.00749$, $S_{12} = -0.00293$, $S_{44} = 0.00859$

The ideal spherical shape of the 3D directional dependence is associated with the isotropic nature of the material, while the non-spherical shape reflects anisotropy. The 3D surfaces with their 2D projections of different planes [100], [010], and [001] for the compressibility modulus, Young's modulus, and shear modulus of the RuAsNb compound are illustrated in Figures 3, 4, and 5, respectively.

According to Figure 3, the compressibility module exhibits a perfect spherical shape in three dimensions (3D), suggesting isotropic behavior for the studied alloy. According to Figures 4 and 5, a significant deviation from the spherical shape can be observed for the shear modulus and Young's modulus, highlighting a significant degree of anisotropy in the shear modulus. In Figures 3, 4, and 5, the 2D projections of the compressibility modulus *B*, Young's modulus *E*, and shear modulus *G* on the (100), (010), and (001) planes exhibit an isotropic character for *B* and a pronounced anisotropic behavior for *G* compared to *E*.

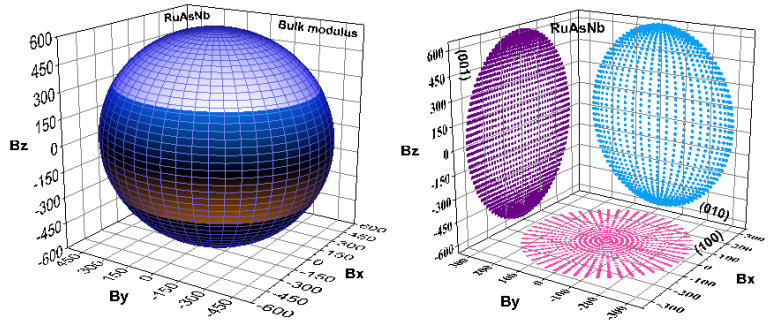

Figure 3. 3D illustration of the bulk modulus, and 2D surface projections on the planes (100), (010), and (001) for the compound RuAsNb

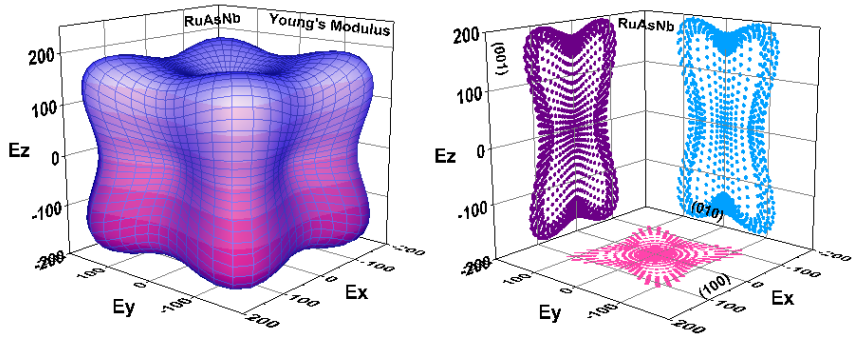

Figure 4. 3D illustration of the Young's modulus, and 2D surface projections on the planes (100), (010), and (001) for the compound RuAsNb

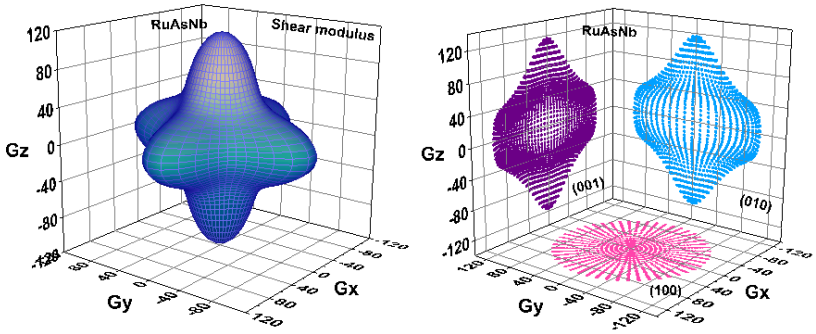

Figure 5. 3D illustration of the shear modulus and 2D surface projections on the planes (100), (010), and (001) for the compound

3.3. Thermoelectric Properties and lattice Thermal Conductivity

We conducted a comprehensive assessment of the thermoelectric properties using semiclassical Boltzmann transport theory within the constant-scattering-time approximation, as implemented in the BoltzTraP code.This approach, grounded in Boltzmann theory **[18],** provides a detailed and accurate perspective on the thermoelectric response of the considered system. The determination of electronic transport properties, including electrical conductivity, Seebeck coefficient, and electronic thermal conductivity, involves using calculated band structures as inputs for the BoltzTraP package **[19].**

For this section, we utilized the band structure calculated using the WC-GGA approximation to compute the thermoelectric properties of the compound RuAsNb.

We will now express the Seebeck coefficient, electrical conductivity, and the electronic transport tensors of thermal conductivity as follows **[20,21]:**

$$S_{\alpha\beta}(T,\mu)=\frac{1}{e\cdot T\cdot\sigma_{\alpha\beta}(T,\mu)}\int\sigma_{\alpha\beta}(\in)\cdot(\in-\mu)^2\left[-\frac{\partial f_0(T,\in,\mu)}{\partial\in}\right], \tag{14}$$

$$\sigma_{\alpha\beta}=\frac{1}{\Omega}\int\sigma_{\alpha\beta}(\in)\left[-\frac{\partial f_0(T,\in,\mu)}{\partial\in}\right]\cdot d\in, \tag{15}$$

$$k^0_{\alpha\beta}(T,\mu)=\frac{1}{e^2\cdot T\cdot.\Omega}\int\sigma_{\alpha\beta}(\in)\cdot(\in-\mu)^2\left[-\frac{\partial f_0(T,\in,\mu)}{\partial\in}\right]\cdot d\in, \tag{16}$$

Where e is the electron charge, Ω is the reciprocal space volume, is the bearer energy, f is the Fermi distribution function, μ is the chemical potential, and T is the absolute temperature.

The conductivity tensor $\sigma_{\alpha\beta}(\in)$ in terms of energy and electronic thermal conductivity k is expressed as:

$$\sigma_{\alpha\beta}(\in)=\frac{1}{N}\sum_{i,k}\sigma_{\alpha\beta}(i,k)\frac{\delta(\in-\in_{i,k})}{d\in}. \tag{17}$$

Where N is the number of k-points.

It is evident within the realm of semiconductor materials that in a p-type semiconductor, the majority charge carriers are identified as holes, while the minority carriers consist of electrons. Conversely, in an n-type semiconductor, electrons are the majority charge carriers, whereas holes are minority carriers. **[22].** This fundamental distinction between the two types of semiconductors underscores the importance of understanding the nature of dominant charge carriers, which is crucial for comprehending the electronic properties and conduction behavior of these materials. In Figure 6, we have depicted the variation of the Seebeck coefficient as a function of chemical potential ranging from [considered as the carrier concentration for the alloys] at different constant temperatures (300, 600, and 900 °K) for our alloy **[23].**

The negative characteristic of the Seebeck coefficient (S) indicates n-type conduction, with electrons as the main charge carriers. Conversely, the positive sign of S implies p-type conduction, with holes as the majority charge carriers.

In this compound, the optimal values of the Seebeck coefficient (S) are observed around the Fermi energy (Ef). Indeed, S is inversely proportional to electrical conductivity, and in this energy range, conduction is intrinsic, resulting in low electrical conductivity. These optimal values tend to decrease as the temperature (T) increases.

Furthermore, it is observed that for this compound, when the value of S is positive, it indicates that the conduction is of P-type. Therefore, this semi-Heusler compound is a p-type semiconductor, as confirmed in the work of Zhenzhen Feng et al **[3]** and also by Fatiha Cherifi et al **[4].**

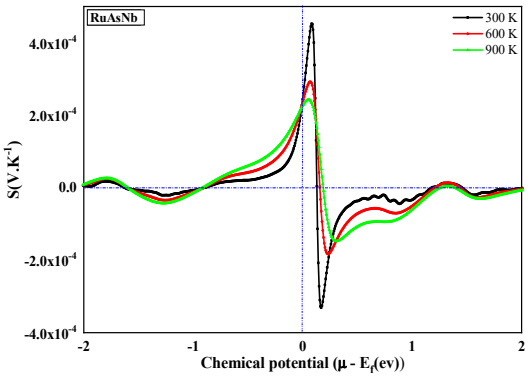

Figure 6. Seebeck coefficient S as a function of chemical potential μ

Figure 7 illustrates the variation of electrical conductivity as a function of chemical potential $\mu-E_F=\pm 2eV$ at different temperatures (300°K, 600°K, and 900°K). This curve highlights that the effect of temperature on electrical conductivity is negligible.

Regarding electronic thermal conductivity, Figure 8 clearly shows that an increase in temperature leads to a marked rise in the electronic thermal conductivity of our compound. Furthermore, the electronic thermal conductivity curve exhibits a shape similar to that of the electrical conductivity curve, suggesting that charge carriers also play a crucial role as heat carriers **[24].**

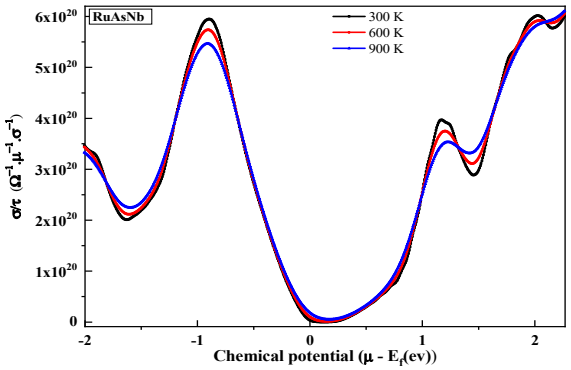

Figure 7. Electrical conductivity σ / τ as a function of chemical potential μ

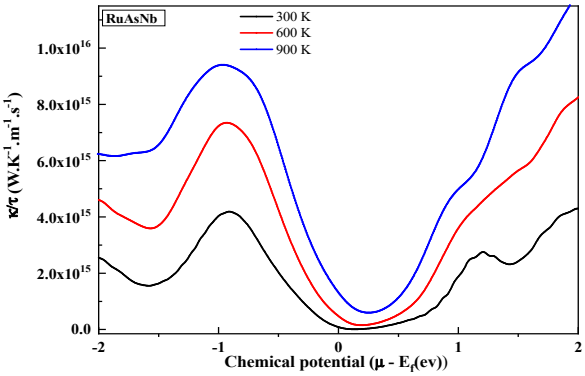

Figure 8. Electronic thermal conductivity k / τ as a function of chemical potential μ

The performance of a thermoelectric material is assessed using a dimensionless parameter called the figure of merit, denoted as *ZT*. This quantifies the enhancement of the thermoelectric performance of a material and can be calculated using the following formula **[25,26]**:

$$ZT = \frac{S^2 \cdot \sigma}{k_e + k_l} \cdot T \,. \tag{18}$$

Where: T the absolute temperature, S is the Seebeck coefficient, σ s the electrical conductivity, k_e is the electronic thermal conductivity, and k_l is the lattice thermal conductivity.

We calculated the variation of the figure of merit ZT as a function of chemical potential over an extended temperature range to assess if the system can maintain favorable thermoelectric performance even at elevated temperatures. A figure of merit ZT equal to or greater than unity indicates excellent transport properties.

In Figure 9, *ZT* is maximal at a temperature of 300 K only at the peaks, but as soon as *ZT* starts to decline, the values at the highest temperature (900 K) dominate compared to the temperature of 300 K.

The values of the figure of merit associated with the Half Heusler RuAsNb are attributed to their low levels of electrical conductivity, combined with their high thermal conductivity. The value *ZT* of the compound is approximately 0.869 at ambient temperature.

In Figure 10, depicting the power factor as a function of chemical potential, an increase in *PF* is observed with the rise in temperature, reaching a maximum value at T=900°C. Two peaks of high intensity are also notable, with one being a primary peak near the Fermi level boundary, having a value of 1.2973×1012 W K^2/ms.

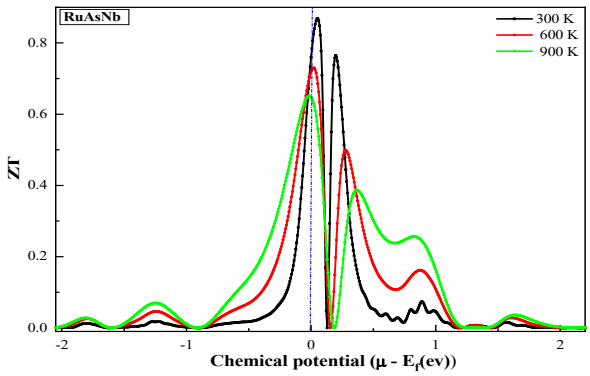

Figure 9. The merit factor, (ZT) as a function of the chemical potential μ

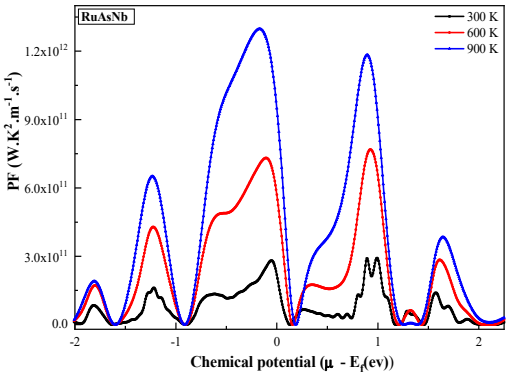

Figure 10. The power factor (*PF*) as a function of the chemical potential μ

The lattice thermal conductivity (k_l) of this compound is determined using Slack method **[27]**. The lattice thermal conductivity is given as:

$$k_l = A \cdot \frac{M \cdot \theta_D^3 \cdot \delta}{\gamma \cdot n^{\frac{2}{3}} \cdot T} \,. \tag{19}$$

Where n is the number of atoms in the primitive unit cell, δ^3 is volume per atom, θ_D is the Debye temperature M is the average mass of atoms, T is an absolute temperature, γ is Grüneisen parameter. The constant A is collection of physical constants, which is determined as:

$$A = \frac{5.20 \cdot 0.847 \cdot 10^7}{2.\left[1 - \left(\frac{0.514}{\gamma}\right) + \left(\frac{0.228}{\gamma^2}\right)\right]}. \tag{20}$$

Further γ is calculated using Poison ratio ν by using following formula

$$\gamma = \frac{3 \cdot (1+\nu)}{2 \cdot (2-3\nu)}. \tag{21}$$

The thermal conductivity of the lattice in this compound varies with temperature, as shown in Figure 11. An increase in temperature leads to a decrease in the thermal conductivity of this material. At 300 K, the lattice thermal conductivity of RuAsNb is 35.01 $W \cdot K^{-1} \cdot m^{-1}$. Comparing our value to the one calculated by Fatiha Cherifi et al. **[4],** which is 15.2 $W \cdot K^{-1} \cdot m^{-1}$, our value is significantly higher, approaching nearly twice that of the latter

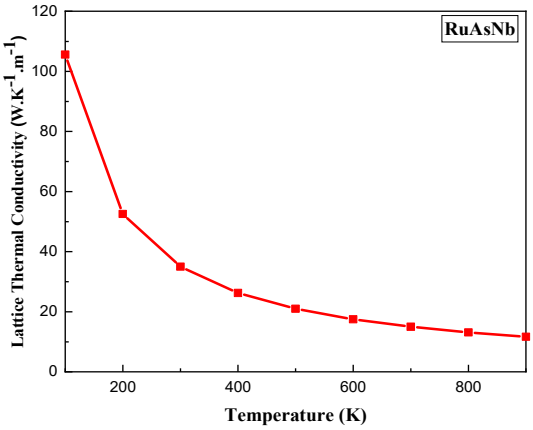

Figure 11. The variation of lattice thermal conductivity as function of temperature for RuAsNb

4. CONCLUSIONS

In this investigation, we employed the Full-Potential Linearized Augmented Plane Wave (FP-LAPW) method, as implemented in the WIEN2k software, to thoroughly investigate the structural, electronic, optical, and thermoelectric properties of the RuAsNb compound. By utilizing the TB-mBJ potential, we calculated the electronic band structure, which revealed an energy gap consistent with experimental observations.

Our analysis highlighted the material's advantageous optical properties, suggesting its potential applicability across the infrared, visible, and ultraviolet regions of the electromagnetic spectrum. Furthermore, we assessed the thermoelectric characteristics of RuAsNb, focusing on key parameters such as the Seebeck coefficient, as well as electrical and thermal conductivities, and the power factor. Notably, our findings confirmed that holes are the dominant charge carriers, establishing RuAsNb as a p-type semiconductor.

We also explored the influence of variations in chemical potential on the thermoelectric properties, providing valuable insights into their temperature-dependent behavior. To enhance the robustness of our conclusions, we conducted a comparative analysis across various exchange–correlation potentials. The promising optical and thermoelectric properties of RuAsNb underscore its potential as a candidate for next-generation energy devices and photovoltaic applications. Collectively, these findings contribute significantly to the understanding of the applicability of RuAsNb in advanced materials for energy conversion technologies.

ORCID

Amraoui Rabie, https://orcid.org/0000-0001-9256-488X

REFERENCES

[1] S. Kadri, T. Mohamed, B. Mahièddine, A. Rabie, and B. Zeyneb, "Study of Structural, Elastic, Thermal and Transport Properties of Ternary X(X=Co, Rh and Ir)MnAs Obtained by DFT," East European Journal of Physics, (1), 47–57 (2022). https://doi.org/10.26565/2312-4334-2022-1-07

[2] Z. Feng, Y. Fu, P. Aditya, Y. Zhang, and D.J. Singh, "Electronic Structure as a Guide in Screening for Potential Thermoelectrics: Demonstration for Half-Heusler Compounds," Physical Review, **100**(8), 085202 (2019). https://doi.org/10.1103/PhysRevB.100.085202

[3] Z. Feng, Y. Fu, Y. Zhang, and D.J. Singh, "Characterization of Rattling in Relation to Thermal Conductivity: Ordered Half-Heusler Semiconductors," Physical Review, **101**(6), 064301 (2020). https://doi.org/10.1103/PhysRevB.101.064301
[4] F. Cherifi, Z. Mostefa, A. Boukra, Z.F. Meghoufel, M. Bouattou, F.K. Allah, and F. Terki, "Thermoelectric Transport Parameters of P-Type RuVAs and RuNbAs Heusler Alloys," Physica Status Solidi (b), basic solid state physics, **257**(12), 2000271 (2020). https://doi.org/10.1002/pssb.202000271
[5] P. Blaha, K. Schwarz, G.K.H. Madsen, D. Kvasnicka, J. Luitz, R. Laskowski, F. Tran, *et al*., *WIEN2k: An Augmented Plane Wave Plus Local Orbitals Program for Calculating Crystal Properties*, (Techn. Universitat, Vienna, 2019).
[6] W. Kohn, and L.J. Sham, "Self-Consistent Equations Including Exchange and Correlation Effects," Physical Review Journals Archive, **140**(4A), 1133–1138 (1965). https://doi.org/10.1103/PhysRev. 140.A1133
[7] F.D. Murnaghan, "The Compressibility of Media under Extreme Pressures," Physics, **30**(9) 244–247 (1944). https://doi.org/10.1073/pnas.30.9.244
[8] S. Bouaricha, R. Kadrib, A. Amraoui, A. Boumaza, M. Belkhiri, F.E.Z. Tourab, D. Rahmaoui, *et al*., "DFT Calculation of Physical Properties for Performance Comparison of Electrothermal Actuators Made of Polysilicon and FeAsNb Alloy," Physics of the Solid State, **67**(9), 821-834 (2025). https://doi.org/10.26565/2312-4334-2022-1-07
[9] D. Behera, B. Akila, R. Amraoui, S. Kadri, S.K. Mukherjee, M.M. Salah, and A. Saeed, "Excellent Thermoelectric Performance in KBaTh (Th = Sb, Bi) Based Half-Heusler Compounds and Design of Actuator for Efficient and Sustainable Energy Harvesting Applications," Crystals, **13**(11), 1551 (2023). https://doi.org/10.3390/cryst13111551
[10] F. Tran, and P. Blaha, "Accurate Band Gaps of Semiconductors and Insulators with a Semilocal Exchange-Correlation Potential," Physical Review Letters, **102**(226401), 1–3 (2009). https://doi.org/10.1103/PhysRevLett.102.226401
[11] M. Born, and K. Huang, *Dynamical Theory of Crystal Lattices*, (Clarendon Press Publication, Oxford, 1998); R.Hill, "The Elastic Behaviour of a Crystalline Aggregate," Proceedings of the Physical Society. Section A, **65**(5), 349–354 (1952). https://doi.org/10.1088/0370-1298/65/5/307
[12] S. Pugh, "XCII. Relations between the elastic moduli and the plastic properties of polycrystalline pure metals," The London, Edinburgh, and Dublin Philosophical Magazine and Journal of Science, **45**(367), 823–843 (1954). https://doi.org/10.1080/14786440808520496
[13] Y. Tian, B. Xu, Z. Zhao, "Microscopic Theory of Hardness and Design of Novel Superhard Crystals," International Journal of Refractory Metals and Hard Materials, **33**, 93–106 (2012). https://doi.org/10.1016/j.ijrmhm.2012.02.021
[14] V. Razumovskiy, E. Isaev, A. Ruban, and P. Korzhavyi, "Ab initio calculations of elastic properties of Pt–Sc alloys," Intermetallics, **16**(8), 982–986 (2008). https://doi.org/10.1016/j.intermet.2008.04.016
[15] N. Arıkan, A. İyigör, A. Candan, Ş. Uğur, Z. Charifi, H. Baaziz, and G. Uğur, "Electronic and phonon properties of the full-Heusler alloys X2YAl (X = Co, Fe and Y = Cr, Sc): a density functional theory study," Journal of Materials Science, **49**, 4180-4190 (2014). https://doi.org/10.1007/s10853-014-8113-7
[16] H. Inaba, and T. Yamamoto, "Debye Temperature of Materials," Netsu Sokutei, **10**, 132–145 (1983).
[17] E. Bringuier, "The Boltzmann equation and relaxation-time approximation for electron transport in solids," European Journal of Physics, **40**, 1–33 (2019). https://doi.org/10.1088/1361-6404/aaf5f0
[18] G.K.H. Madsen, and D.J. Singh, "BoltzTraP. A code for calculating band-structure dependent quantities," Computer Physics Communications, **175**(1), 67–71 (2006). https://doi.org/10.1016/j.cpc.2006.03.007
[19] G. Snyder, in: *CRC Handbook of Thermoelectrics*, edited by D.M. Rowe, (CRC Press, Boca Raton, 2006). p. 144.
[20] B. Lenoir, *Thermoélectricité: des principes aux applications*, (Transport, 1990). pp. 1–19.
[21] X. Zhang, and J. Xia, "Approaches to design inorganic semiconductors while maintaining structural motifs," Journal of Semiconductors, **39**(7), 1 (2018). https://doi.org/10.1088/1674-4926/39/7/071002
[22] T.J. Seebeck, *Magnetic Polarization of metals and minerals*, (Abhand. Deut. Akad. Wiss, Berlin, 1822).
[23] M.J. Winiarski, K. Bilinska, K. Ciesielski, and D. Kaczorowski, "Thermoelectric performance of p-type half-Heusler alloys ScMSb (M=Ni, Pd, Pt) by ab initio calculations," Journal of Alloys and Compounds, **762**, 901–905 (2018). https://doi.org/10.1016/j.jallcom.2018.05.257
[24] P. Taylor, and C. Wood, "Thermoelectric properties of Ag_2Te and Ag_2Se," Adv. Energy Convers. **01**, 141–145 (1961). https://doi.org/10.1016/0365-1789(61)90023-6
[25] R. Amraoui, S. Kadri, H. Meradji, M. Berkani, A. Bouaricha, S. Ghemid, A. Boumaza, *et al*., "First-principles computational study on structural, elastic, magnetic, electronic, and thermoelectric properties of Co_2MnGe: a potential Heusler ternary compound," The European Physical Journal B, **95**, 1–14 (2022). https://doi.org/10.1140/epjb/s10051-022-00466-y
[26] G.A. Slack, "The Thermal Conductivity of Nonmetallic Crystals," Solid state physics, **34**, 1–71 (1979). https://doi.org/10.1016/s0081-1947(08)60359-8

ДОСЛІДЖЕННЯ ЕЛЕКТРОННИХ, ПРУЖНИХ ТА ТРАНСПОРТНИХ ВЛАСТИВОСТЕЙ МЕТОДОМ DFT, І ОЦІНКА ҐРАТКОВОЇ ТЕПЛОПРОВІДНОСТІ НАПІВГЕЙСЛЕРОВОГО СПЛАВУ RuAsNb

Азіза Бутута[1], Амор Буаріча[2,5], Ф. Зеніхері[3,7], Зейнеб Борджиба[4], Рабі Амрауї[3,4], Салім Кадрі[5,6], Валід Бенджедду[6], Салах Агіб[6]

[1]Центр досліджень механіки CRM, По. Box 73 B, 25021, Константіна, Алжир
[2]Наукова зона Університету Гардайя, PO Box 455, Гардайя, 47000, Алжир
[3]Вища нормальна школа технологічної освіти, Скікда, 21000, Алжир
[4]Лабораторія фізики матеріалів - L2PM, Університет Гельма 8 травня 1945 р. Алжир
[5]Лабораторія промислової механіки (LMI), Баджі Мохтар — Університет Аннаба, PO Box 12, Аннаба, 23000, Алжир
[6]Лабораторія динаміки двигунів та віброакустики (LDMV), Університет М'хамеда Бугерра, Бумердс, 35000, Алжир
[7]Лабораторія активних компонентів і матеріалів, Університет Ларбі Бен М'Хіді, Ум Ель Буагі, 04000, Алжир

У цьому дослідженні ми застосували метод повнопотенціальної лінеаризованої доповненої плоскої хвилі (FP-LAPW), реалізований у Wien2k, для проведення комплексного дослідження структурних, електронних та термоелектричних властивостей RuAsNb. Електронна зонна структура була розрахована з використанням обмінно-кореляційного потенціалу

TB-mBJ, що призвело до енергетичної забороненої зони, яка добре узгоджується з наявними експериментальними даними. Крім того, наш аналіз виявив сприятливі оптичні властивості, що підкреслює потенціал матеріалу для застосування в інфрачервоному, видимому та ультрафіолетовому діапазонах електромагнітного спектру. Ми також оцінили термоелектричні характеристики RuAsNb, проаналізувавши ключові параметри, зокрема коефіцієнт Зеєбека, електропровідність, теплопровідність та коефіцієнт потужності. Результати показують, що дірки є домінуючими носіями заряду, що підтверджує напівпровідникову природу p-типу RuAsNb. Крім того, було досліджено вплив змін хімічного потенціалу на ці термоелектричні властивості, що дало цінну інформацію про їх температурно-залежну поведінку. Щоб забезпечити надійність наших висновків, було проведено порівняльне дослідження з використанням різних обмінно-кореляційних потенціалів, яке додатково підтвердило узгодженість результатів. Перспективні термоелектричні характеристики RuAsNb свідчать про його придатність як потенційного кандидата для пристроїв перетворення енергії наступного покоління та фотоелектричних застосувань. Більше того, оцінка теплопровідності решітки за допомогою моделі Слака підвищує надійність наших прогнозів та надає цінні знання для майбутніх досліджень. Загалом, ця робота сприяє глибшому розумінню потенціалу RuAsNb у передових енергетичних матеріалах.

Ключові слова: *напівгейслер; DFT; структурна властивість; анізотропія; оптичні властивості; показник якості*